A simple cell model with dominating opponent inhibition for robust contrast detection

Thorsten Hansen, Gregory Baratoff, Heiko Neumann

Universität Ulm, Fakultät für Informatik, Abt. Neuroinformatik, D-89069 Ulm (e-mail:{hansen, baratoff, hneumann}@neuro.informatik.uni-ulm.de)

Ein Modell kortikaler Einfachzellen mit dominanter opponenter Inhibition zur robusten Kontrastdetektion

Zusammenfassung. Im primären visuellen Pfad wird Information in zwei getrennten, komplementären Domänen repräsentiert, den on- und off-Zellen. In dieser Arbeit untersuchen wir die Interaktion von on- und off-Zellen zur Generierung der Eingabe für eine kortikale Einfachzelle. Basierend auf physiologischen Studien schlagen wir einen Mechanismus vor, bei dem eine kortikale Einfachzelle aus beiden Domänen eine Eingabe erhält, wobei die Eingabe aus dem opponenten Pfad stärker gewichtet wird. Mit diesem Mechanismus der dominanten opponenten Inhibition können Antworten von kortikalen Einfachzellen auf Hell-Dunkel-Balken simuliert werden, die im primären visuellen Kortex der Katze gemessen wurden. Bei der Verarbeitung synthetischer und natürlicher Bilder können mit dem neuen Modell schärfere Antworten und bessere Rauschunterdrückung erreicht werden. Wir geben eine stochastische Analyse der Rauschunterdrückungscharakteristika des vorgeschlagenen
Mechanismus und präsentieren detaillierte numerische Simulationen mit systematischen Parametervariationen. Die Resultate zeigen, dass das Modell kortikaler Einfachzellen mit dominanter opponenter Inhibition robuster gegenüber verrauschten Eingaben wird, weitgehend unabhängig von der Stärke des Rauschens. Diese Eigenschaft ist möglicherweise der Grund für die physiologisch gemessene dominante Inhibition und für die Repräsentation von Kontrastinformation in zwei komplementären Domänen. Basierend auf diesen Ergebnissen stellen wir die Hypothese auf, dass dominante opponente Inhibition im visuellen System verwendet wird, um in verrauschten Umgebungen Kontraste robust extrahieren zu können.

Summary. In the primary visual pathway, information is represented in two distinct, complementary domains, namely "on" and "off" cells. In this work we examine how on and off cells may interact to form the input to simple cell subfields. On the basis of physiological evidence, we propose a mechanism of dominating opponent inhibition, where a simple cell subfield is driven by both on and off domains, receiving more heavily weighted input from the opponent pathway.
We demonstrate that the model can account for physiological data on luminance gradient reversal recorded from simple cells in cat striate cortex. Next, we use the model for the processing of synthetic and natural images, showing that sharpness of response and robustness to noise can be increased by dominating opponent inhibition. Finally, we present a stochastic analysis of the noise-suppression characteristics of the proposed mechanism accompanied by detailed simulations with systematic parameter variations. Results show that dominating opponent inhibition makes the simple cell responses more robust to noise, largely independently of the amount of noise added. This property may give a rationale for the strong inhibition measured physiologically and for the representation of contrast information in two complementary domains. On the basis of these findings, we hypothesize that the visual system uses dominating opponent inhibition in order to robustly extract features in noisy environments.

1 Introduction

Processing of visual stimuli begins in the retina, where electromagnetic radiation within a certain frequency band is transformed into a neural code. The first major processing stage consists of retinal ganglion cells with center-surround receptive fields (RFs). Axons of ganglion cells form the optic nerve, which terminates in a relay structure of the thalamus, the lateral geniculate nucleus (LGN). LGN cells project upon the primary visual area V1 in the occipital lobe. Here, simple cells are found with an RF structure that is different from that of the ganglion cells. Simple cells have elongated RFs and respond to bars of a certain orientation and position.

Several schemes have been proposed for the neural wiring of LGN cell afferents to subfields of simple cells. In the classical proposal of Hubel and Wiesel (1962), excitatory signals from on cells drive the on subfield, whereas excitatory signals from off cells drive the off subfield (Fig. 1a). Another approach assumes that simple cells are driven by one type of ganglion cells alone Heggelund (1986). In this case, on-cell signals excite the on subfield and inhibit the off subfield (Fig. 1b).
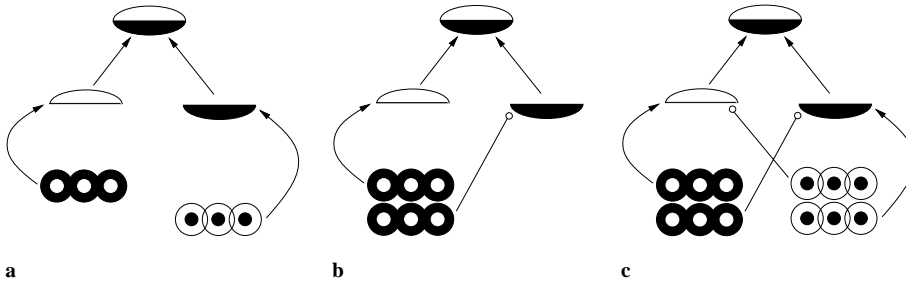
An alternative scheme of opponent inhibition has been proposed by Ferster (1989), in which the on subfield receives excitatory input from the on path and inhibitory input from the off path. The reverse holds true for the off subfield (Fig. 1c). This scheme is employed in a computational model of brightness perception (Pessoa et al. 1995; Neumann et al. 1998) and is investigated regarding its signal processing properties, in particular its scale-space behavior (Neumann et al. 1999). Here, we extend this scheme and introduce an imbalance of excitatory and inhibitory inputs, namely a greater weighting of inhibitory inputs in either subfield. The assumption of strong inhibitory input to a simple cell that can overwhelm excitatory contributions is supported by physiological evidence both from extracellular (Heggelund 1981; Palmer and Davis 1981) and intracellular recordings (Ferster 1988; Borg-Graham et al. 1998; Hirsch et al. 1998). With this mechanism of dominating opponent inhibition (DOI), the model (1) reproduces physiological data of simple cell responses to luminance gradient reversal, and (2) is more robust to noise than a model with balanced excitation and inhibition.

The paper is organized as follows. Section 2 gives a brief overview of the equations defining the model and formally introduces the mechanism of dominating opponent inhibition. In Sect. 3 we simulate a physiological study by Hammond and MacKay (1983) on simple cell responses recorded in cat striate cortex. We show that DOI is the crucial mechanism in our model to reproduce the data. In Sect. 4 we apply the same model with identical parameter settings to noisy synthetic images and real images. We compare the results to simulations without DOI and show that response to noise is significantly reduced for the model with DOI. Finally, in Sect. 5 we investigate the noise suppression properties of the model by a stochastic analysis and by simulating the response of the model to two synthetic test cases (a noisy homogeneous region and a noisy edge) under systematic parameter variations. Section 6 concludes the paper.

2 The model

In this section, we give a short, formal description of the model. Further details can be found in Neumann et al. (1999). The model consists of a hierarchical organization of two main processing stages, namely on and off cells, followed by a simple cell circuit. In all equations, Greek letters denote positively valued model parameters.
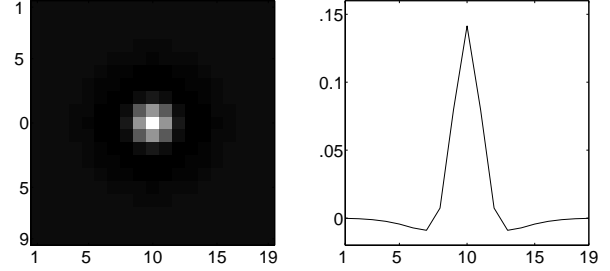

Fig. 2. Left: DoG filter mask used for modeling the on and off cells; right: the corresponding horizontal cross-section taken at the center of the mask

2.1 LGN cells

The input luminance distribution is given by a stimulus I, with luminance values normalized to the range $[0; 1]$. Responses of isotropic LGN cells are modeled by convolution of the input stimulus I with a difference of Gaussians (DoG) operator. LGN on and off cell activities X_{on} and X_{off} are modeled as rectified positive or negative DoG responses, respectively:

$$X = \mathrm{DoG}_{\sigma_c, \sigma_s} * I \ , \tag{1}$$

$$X_{\mathrm{on}} = [X]^+ \ , \qquad X_{\mathrm{off}} = [-X]^+ \ , \tag{2}$$

where $*$ is the spatial convolution operator and $[x]^+ := \max\{x, 0\}$ denotes half-wave rectification. The DoG is given by the difference of a center Gaussian with small standard deviation $\sigma_c = 1$ and a surround Gaussian with larger standard deviation $\sigma_s = 3$:

$$\mathrm{DoG}_{\sigma_c, \sigma_s} = G_{\sigma_c} - G_{\sigma_s}. \tag{3}$$

The Gaussians are sampled within a 3σ interval, resulting in a filter mask of size 19×19 ($3\sigma_s \times 2 + 1 = 19$). Figure 2 shows the filter mask of the DoG operator together with a horizontal cross-section.

2.2 Simple cells

The next processing stage deals with simple cells, which are modeled for eight discrete orientations $\theta = 0°, 22.5°, 45°, \ldots, 157.5°$ and for two opposite contrast polarities, namely, light-dark and dark-light.
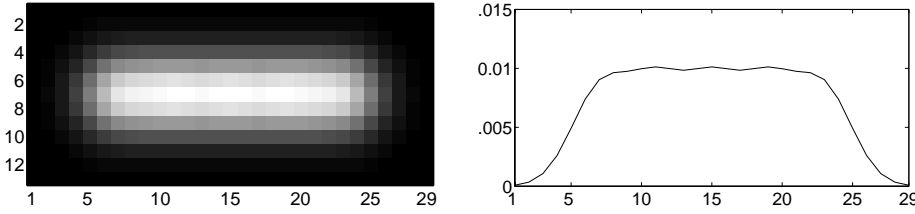
Fig. 3. **Fig. 3.** Left: Filter mask for a simple cell subfield of orientation $0°$; right: the corresponding horizontal cross-section taken at the center of the mask

2.2.1 Simple cell subfields with dominating opponent inhibition

A simple cell has two adjacent subfields, an on subfield sensitive to light increments and an off subfield sensitive to light decrements. Simple cell subfields are defined by elongated, oriented weighting functions G_θ (Fig. 3). The weighting function G_θ is modeled with five isotropic Gaussians with $\sigma = 2$, which are properly aligned along the preferred axis of orientation θ and spaced within a distance of two standard deviations. This results in a plateau-like RF which is $29/19 \approx 1.5$ times larger than the RF of the on and off cells. Generally, for N Gaussians with a standard deviation σ, the length of the filter mask is given by $(N-1)2\sigma + 2 \cdot 3\sigma + 1$.

Before integration, contrast activity of different polarity competes at each spatial location. Input activation for both on and off subfields R_{on} and R_{off} with a preferred orientation θ is computed by convolution of the weighted difference of unoriented LGN responses X_{on} and X_{off} with the subfield mask G_θ of the same orientation preference:

$$R_{on,\theta} = [(X_{on} - \xi X_{off}) * G_\theta]^+,$$
$$R_{off,\theta} = [(X_{off} - \xi X_{on}) * G_\theta]^+. \qquad (4)$$

The case of equally weighted on and off inputs occurs for $\xi = 1$. The newly proposed scheme of dominating opponent inhibition (DOI) introduces $\xi > 1$; which scales up the opponent contribution. This introduces a "one against many" situation, where, e.g., an on subfield only receives input if the contribution of the on channel X_{on} is ξ times larger than the contribution of the opponent off channel X_{off}. DOI processing has important effects on the behavior of the model: it is the key feature for simulating data in a physiological study on luminance gradient reversal (Sect. 3), and it makes the model more robust to noise (Sects. 4 and 5).

2.2.2 Nonlinear simple cell circuit

On and off subfields interact via a disinhibition circuit that boosts activities for spatially juxtaposed on and off contrast configurations. Such juxtaposed on and off contrasts occur at step edges, thus the simple cell model exhibits significantly higher responses for this configuration than for shallow luminance gradients, for example.

The circuit that defines the simple cell model comprises three intermediate stages, namely, $S^{(1)}$, $S^{(2)}$, and $\widetilde{S}$ (Fig. 4). The various connections and their different computational roles are explained in the following. A comprehensive description and a detailed motivation of the nonlinear simple cell circuit are given by Neumann et al. (1999). The basic circuitry is given by the excitatory $R_{on/off} \to S^{(2)}_{on/off} \to \widetilde{S}$

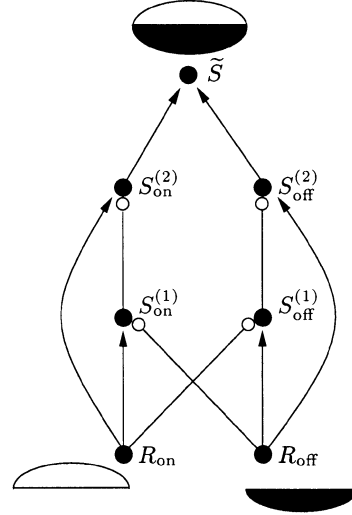**Fig. 4.** Sketch of the simple cell circuit. *Arrows* denote the excitatory input, *circles* at the end of lines denote inhibitory input. Index θ is omitted to simplify notation

connections, which define the excitatory input to the simple cell from its two subfields R_{on} and R_{off}. A model having only this basic circuitry results in a simple cell that linearly sums its input. To make the model more selective for juxtaposed on and off contrasts, additional connections are introduced. The on-channel path $R_{on} \to S^{(1)}_{on} \multimap S^{(2)}_{on}$ implements a self-normalization by inhibition of $S^{(2)}_{on}$, which prevents arbitrarily large activity in the cell. The same holds true for the off channel. The key connections of the model are the cross-channel inhibitory connections $R_{on} \multimap S^{(1)}_{off}$ and $R_{off} \multimap S^{(1)}_{on}$. By disinhibition, i.e., inhibiting the inhibition of $S^{(1)}$, the simple cell response is nonlinearly amplified if both subfields are active simultaneously.

The first two stages are steady-state solutions of inhibitory shunting interactions. The equations for the on channel read

$$S^{(1)}_{on} = \frac{R_{on}}{\alpha_S + \beta_S R_{off}},$$
$$S^{(2)}_{on} = \frac{R_{on}}{\gamma_S + \delta_S S^{(1)}_{on}}.$$

The corresponding equations for the off channel are obtained by interchanging on and off. Here and in the remainder of this section, variables occur for all discrete orientations. The index θ is omitted to simplify notation. The activity of the third stage $\widetilde{S}$ results from pooling the contributions of the on and off channel

$$\widetilde{S} = S^{(2)}_{on} + S^{(2)}_{off}.$$

Combining these equations and assuming a symmetric relation between the two channels by setting $\delta_S = \beta_S \gamma_S$
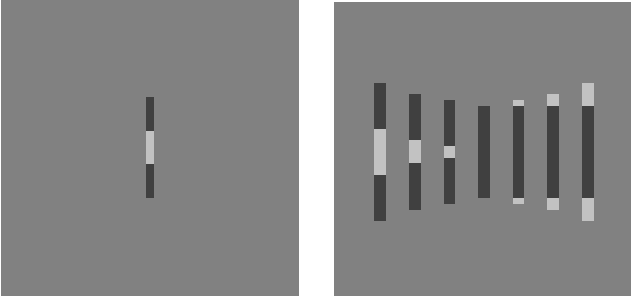
Fig. 5. Example of stimulus used (left) and a set of stimuli for a fixed length of the dark bar (right)

yields a more concise equation. The resulting simple cell activity consists of a linear and a nonlinear, i.e., multiplicative, term

$$\widetilde{S} = \frac{\alpha_S(R_{\mathrm{on}} + R_{\mathrm{off}}) + 2\beta_S(R_{\mathrm{on}}R_{\mathrm{off}})}{\alpha_S\gamma_S + \beta_S\gamma_S(R_{\mathrm{on}} + R_{\mathrm{off}})}. \qquad (5)$$

The parameters are set to $\alpha_S = 1.0$, $\beta_S = 10\,000.0$, and $\gamma_S = 0.01$. Their specific choice is not critical as long as the linear components scaled by α_S and γ_S are small compared to the nonlinear component scaled by β_S.

Simple cells sensitive to opposite contrast polarity, i.e., light-dark and dark-light, finally undergo mutual inhibition, which sharpens the activity profile:

$$S_{\mathrm{ld}} = \left[\widetilde{S}_{\mathrm{ld}} - \widetilde{S}_{\mathrm{dl}}\right]^+,$$
$$S_{\mathrm{dl}} = \left[\widetilde{S}_{\mathrm{dl}} - \widetilde{S}_{\mathrm{ld}}\right]^+. \qquad (6)$$

Light-dark and dark-light simple cells are obtained by sampling the subfield activity with different offsets $\pm\tau = 3$ orthogonal to the axis of orientation of the simple cell: a light-dark cell has an on subfield with an offset to the left and an off subfield with an offset to the right. For a dark-light simple cell, left and right offsets are interchanged.

To sum up, the present simple cell model comprises two mechanisms with complementary functionality: DOI serves to suppress undesired spurious activity to noisy inputs, while the nonlinear simple cell circuit sharpens and amplifies desired responses to edges.

3 Simulation of the Hammond and MacKay study

In order to demonstrate the physiological plausibility and relevance of the proposed model, basic properties of simple cells found in vivo are simulated. In particular, we simulate a study of Hammond and MacKay (1983), who investigated the response of simple cells in the cat to optimally oriented bars. This study is challenging for any model of simple cells because it shows the classical effect of linear contrast summation up to saturation as well as strong, possibly nonlinear, suppressive effects (non-classical).

In their study, Hammond and MacKay recorded simple cell responses to three types of bar stimuli: dark bars, dark bars with light segments added in the middle (DLD), and dark bars with light segments added at both ends (LDL).

Figure 5 depicts the single stimulus used and a sample of the whole stimulus set. A main result of their work is shown in Fig. 6. For bar stimuli, linear response up to saturation is observed ('length-summation curve'). When light segments are added to the dark bars (DLD and LDL), the average response decrement is much larger than predicted from linear contrast summation. Linear summation would suggest that the slopes of the length-summation curve and of the LDL and DLD curves are the same.

Our model predicts that simple cell responses as observed by Hammond and MacKay can be generated on the basis of the proposed DOI scheme. Results are shown in Fig. 6 (right). The same model parameters as for the processing of images in Sect. 4 are employed. The declining slopes of the curves for both DLD and LDL stimuli are much steeper than the ascending slope of the length-summation curve, as reported by Hammond and MacKay. In summary, a good qualitative fit with the physiological data is obtained. Note that for the nondominant case, i.e., setting the DOI parameter $\xi = 1$, no strong suppression occurs, but the responses for LDL and DLD bar stimuli lie on the dotted line as predicted by linear contrast summation. To rule out effects of the nonlinear simple cell, the circuit is replaced by a linear model. For the linear model, subfield responses are simply added: $\widetilde{S} = R_{\mathrm{on}} + R_{\mathrm{off}}$, instead of the nonlinear interaction in Eq. 5. For the linear model with DOI, the results obtained are qualitatively the same.

In their paper, Hammond and MacKay speculated that nonlinear or shunting suppression might cause the observed behavior. Considering the results mentioned here, this notion cannot be rejected, but our model shows that a linear mechanism is also sufficient to explain the data.

4 Processing of images

In this section, we show the performance of the model on synthetic and natural images. The values of the model parameters are as described in Sect. 2 and are the same in all simulations. In the simulations, we compare the new mechanism of DOI (setting $\xi = 2$) to a linear simple cell model and to the nonlinear model without DOI ($\xi = 1$). The linear model approximates filtering with a first order Gaussian derivative (Neumann et al. 1999). The edge images shown are obtained by summing up simple cell responses of both contrast polarities for all orientations.

In the first experiment, we employ a synthetic image of a dark ellipse on a lighter background, corrupted with 50% additive Gaussian noise. Figure 7 shows the input stimulus and the simulation results. For this stimulus, we also combined the DOI interaction with a linear model. All models show responses at the edge locations, but only the nonlinear models have a pronounced unimodal response to an edge. Moreover, the results show that the models with DOI are considerably less sensitive to noise. Simulation results for this stimulus exemplify the complementary properties of DOI and of the nonlinear simple cell circuit: DOI serves to suppress noisy inputs, while the nonlinear interaction sharpens the responses to edges.

A further challenge to the model is posed by processing of natural images. We use the tree image shown in Fig. 8.
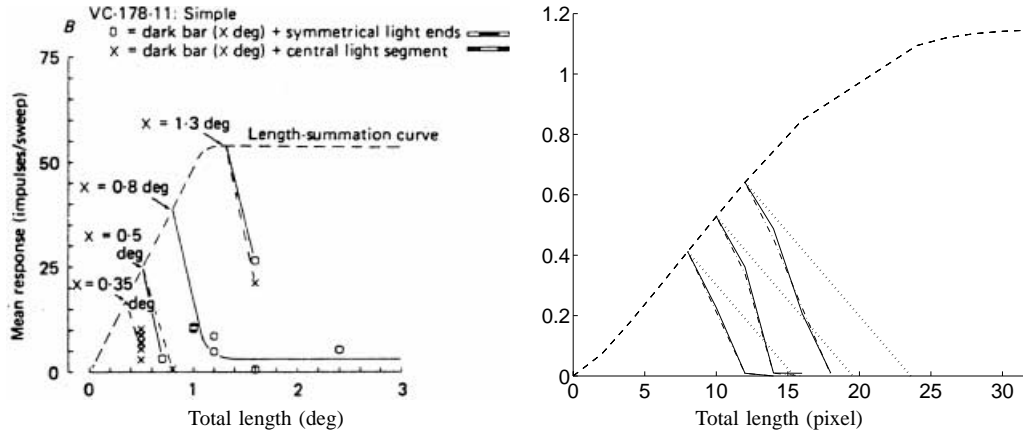
Fig. 6. Results of physiological recordings (left, reprinted from Hammond & MacKay (1983) with permission of the publisher) and simulation (right). Both plots show the length-summation curve (*dashed*) and responses to LDL and DLD bars (*solid* and *dash-dotted*, respectively). For comparison, predictions by linear contrast summation (*dotted*) are shown in the simulation plot

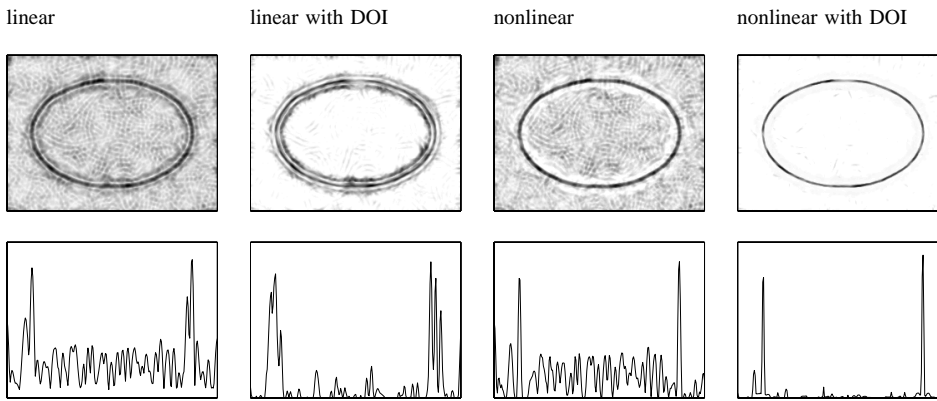linear   linear with DOI   nonlinear   nonlinear with DOI

Fig. 7. Noisy input stimulus and simulation results (top row) together with the corresponding horizontal cross-sections taken at the center of the images (bottom row)

For the DOI processing, responses to the lawn are largely suppressed, while responses to the contour of the tree and to the shadow are enhanced. We also employ an image of a 3D laboratory scene as input stimulus Fig. 9. Here, the contours of the cube are sharper and the spurious responses at the floor vanish for DOI processing.

5 Noise suppression properties

In the previous section, we showed the noise suppression properties of DOI qualitatively. In this section, we clarify the noise suppression properties by a stochastic analysis and by numerical simulations. The stochastic analysis shows that DOI processing introduces an adaptive threshold, using the noise level itself to determine the amount of suppression. As a result, good noise suppression for various noise levels is achieved. In the numerical simulations, we determine the value of the DOI parameter ξ to match two conflicting requirements as well as possible, namely, suppression of noise and responsiveness to edges.

5.1 Stochastic analysis

In this section, we conduct a stochastic analysis of the response properties of DOI to noisy homogeneous regions. Let I be an input image of homogeneous intensity, corrupted by

an additive Gaussian noise process, and let X be the result of applying a DoG filter to I. Because DoG filtering is a linear operation, the resulting X is a Gaussian process as well (Papoulis 1965). At each spatial position, X can be described by a random variable $\mathbf{x}$ with a density $f_{\mathbf{x}}(x)$ that is defined by a Gaussian distribution $g_\sigma(x)$. The DOI interaction in Eq. 4 can be written as

$$\mathbf{y} = \mathbf{x}_{\text{on}} - \xi\,\mathbf{x}_{\text{off}}$$
$$= [\mathbf{x}]^+ - \xi[-\mathbf{x}]^+ = \begin{cases} \mathbf{x} & \text{if } x \geq 0 \\ \xi\mathbf{x} & \text{if } x < 0. \end{cases}$$

The density $f_{\mathbf{y}}(y)$ can be determined with the fundamental theorem on transformations of densities (Papoulis 1965):

$$f_{\mathbf{y}}(y) = \begin{cases} f_{\mathbf{x}}(y) = g_\sigma(y) & \text{if } y \geq 0 \\ 1/\xi\, f_{\mathbf{x}}(1/\xi\,y) = g_{\sigma\xi}(y) & \text{if } y < 0. \end{cases}$$

The next processing step is the convolution of $\mathbf{y}$ with the subfield mask G_θ, which realizes a weighted average over a limited spatial neighborhood. Under the general assumption of an ergodic process (Papoulis 1965), the ensemble (or spatial) average in homogeneous regions corresponds to the mean of the individual units. The mean of $\mathbf{y}$ is given by
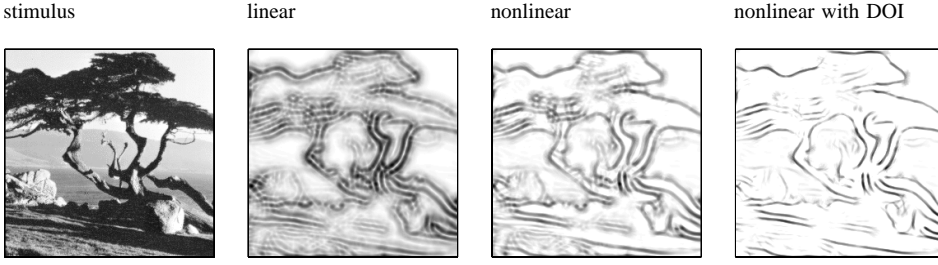
stimulus   linear   nonlinear   nonlinear with DOI

Fig. 8. Natural image of a tree and simulation results

stimulus   linear   nonlinear   nonlinear with DOI

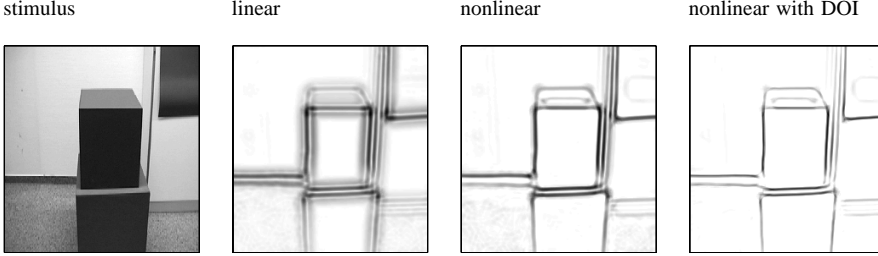**Fig. 9.** Image of a laboratory scene and simulation results

$$E\{\mathbf{y}\} = \int_{-\infty}^{\infty} y f_{\mathbf{y}}(y) \, \mathrm{d}\, y$$

$$= \int_{-\infty}^{0} y g_{\sigma\xi}(y) \, \mathrm{d}\, y + \int_{0}^{\infty} y g_{\sigma}(y) \, \mathrm{d}\, y$$

$$= -\frac{1}{\sqrt{2\pi}} \sigma\xi + \frac{1}{\sqrt{2\pi}} \sigma$$

$$= -\frac{1}{\sqrt{2\pi}} \sigma(\xi - 1). \tag{7}$$

The result shows that the mean is (1) negative for $\xi > 1$ and (2) proportional to the DOI parameter $\xi - 1$ and to the noise level σ. The expression for the mean of $\mathbf{y}$ (Eq. 7) explains the suppression of noise largely independently of the noise level. As the noise level increases, the mean proportionally shifts to more negative values, so that the amount of positive activity left after the subsequent rectification (Eq. 4) remains small. This theoretical finding is confirmed by numerical simulations in the next section (cf. Fig. 10).

5.2 Numerical evaluation

In order to determine the optimal strength of inhibition and to investigate the circuit's response properties to noisy inputs, we measure mean subfield responses R_{on} (Eq. 4). We vary the noise level and the value of the DOI parameter ξ. Simulations are done for two basic situations, namely, noisy homogeneous regions and a noisy step edge. In both cases, Gaussian noise is added to the ideal stimulus.

5.2.1 Noisy homogeneous region

In the first study, a stimulus of homogeneous intensity is corrupted by additive Gaussian noise. We measure the mean response over all spatial positions of an on subfield $\bar{R}_{on,\theta}$. Since noisy homogeneous regions do not have any preferred orientation, the choice of the orientation of the subfield θ is irrelevant. For the simulations, $\theta = 90°$ is chosen.

The results are depicted in Fig. 10 (left). The curves correspond to Gaussian noise of decreasing standard deviations (top to bottom). We observe that the mean subfield response decreases as ξ gets larger and is almost zero for $\xi > \approx 2$. For a more quantitative evaluation, the value of ξ is determined for which the mean subfield response of the respective noise level falls below a certain threshold of $2 \cdot 10^{-5}$ (Fig. 10, right). For the highest noise level, ξ has the value 2.25. The curves show that suppression occurs for values of ξ that are significantly larger than 1, a value which corresponds to balanced excitation and inhibition. Further, suppression is largely independent of the noise level, as only a slight decrease of ξ with the noise level can be observed.

Insight into this adaptive behavior can be gained by analyzing Eq. 4 in more detail. Using Eq. 2 and the equality $[x]^+ - [-x]^+ = x$, we can rewrite Eq. 4 as

$$R_{on,\theta} = [(X_{on} - \xi X_{off})*G_\theta]^+$$

$$= [(X_{on} - X_{off})*G_\theta - (\xi - 1)X_{off}*G_\theta]^+$$

$$= [X*G_\theta - \underbrace{(\xi - 1)X_{off}*G_\theta}_{\text{dynamic threshold}}]^+. \tag{8}$$

This shows that DOI interaction introduces a dynamic threshold that is proportional to ξ and depends on the strength of the signal in the opponent pathway. Note that in the nondominating case for $\xi = 1$, Eq. 8 reduces to

$$R_{on,\theta}|_{\xi=1} = [X*G_\theta]^+ .$$

To summarize, a noisy stimulus generates responses in both on and off pathways. DOI interaction introduces a dynamic threshold by scaling up the contribution of the opponent pathway, which causes a decrease of response proportional to the noise level.

The simulations suggest that any value of $\xi > \approx 2.25$ would be appropriate to suppress responses to noisy homogeneous regions. However, the effect of large ξ to suppress desired responses to signals like edges, for example, also needs to be clarified.
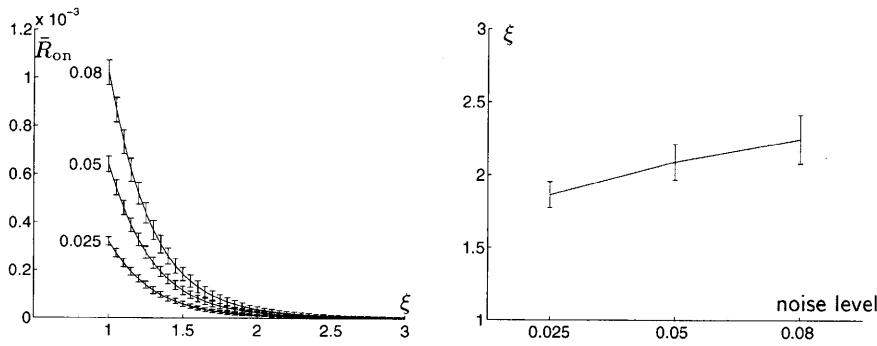
Fig. 10. Left: mean subfield responses $\bar{R}_{\mathrm{on}}$ to homogeneous regions; right: minimal ξ for which the mean subfield response of the respective noise level falls below $2 \cdot 10^{-5}$. For the three noise levels, the respective mean is given by 1.86, 2.09, 2.25. For both plots, three noise levels (standard deviation 0.025, 0.05, 0.08) are employed. Responses are averaged over 100 realizations of the respective noise level; error bars denote ± 1 standard deviation. The curves show that for dominating opponent inhibition with $\xi > \approx 2$, noise is suppressed largely independently of the noise level
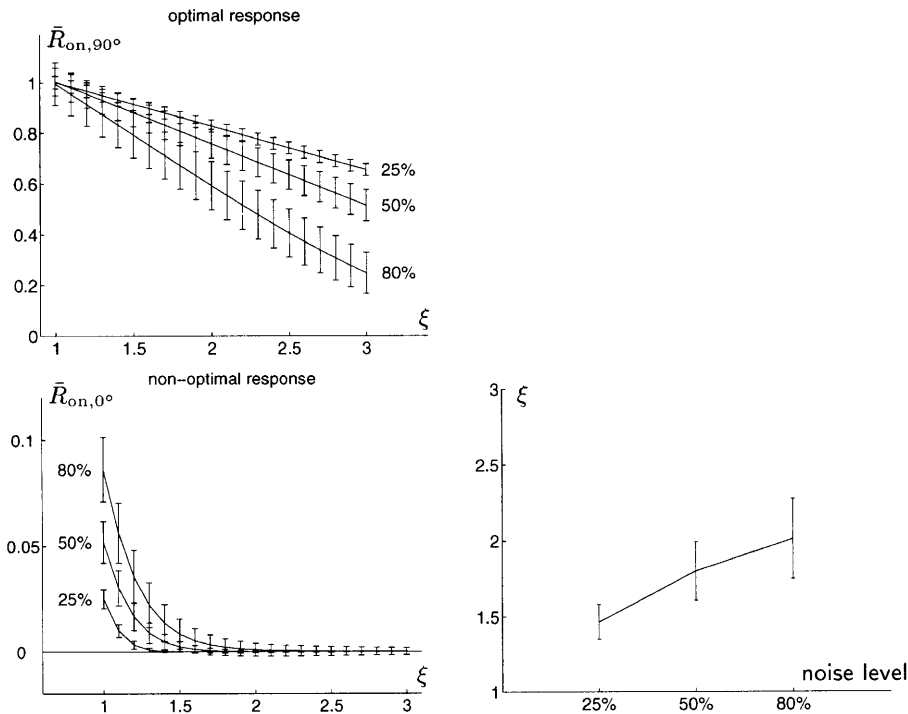

Fig. 11. Mean subfield responses to a noisy step edge, corrupted with 25%, 50%, and 80% additive Gaussian noise for various values of the DOI parameter ξ. Responses are averaged over 100 different realizations of the respective noise level; error bars denote ± 1 standard deviation. Responses are normalized to allow for better comparison. Top left: the mean response of an optimally oriented subfield; bottom left: the mean response of nonoptimally oriented subfield; bottom right: the minimal ξ for which the mean subfield response of the respective noise level is zero. For the three noise levels, the respective means are given by 1.47, 1.80, 2.01. Results show that, for $\xi \approx 2$, nonoptimal responses are almost zero, while the optimal responses are still considerably large

5.2.2 Noisy step edge

In a complementary experiment, an ideal step edge is corrupted with Gaussian noise of the same standard deviations as in the case of noisy homogeneous regions in the previous section. For a luminance difference at the edge of 0.1, this results in 25%, 50%, and 80% Gaussian noise (i.e., noise with a standard deviation of 25%, 50%, and 80% of the luminance difference at the edge). Two kinds of responses are distinguished: response of an optimally oriented subfield $R_{\mathrm{on},90°}$ with an orientation parallel to the edge, and responses of nonoptimally oriented subfields not parallel to the edge. Since all the examined nonoptimal orientations

of 0°, 45°, and 135° yield comparably large responses, we choose one representative, namely, the orthogonal orientation $R_{\mathrm{on},0°}$. For both the optimal and the nonoptimal orientations, we measure the mean response of $R_{\mathrm{on},\theta}$ along a line parallel to the edge. The horizontal position of the line is analytically determined as the position of maximal response of an optimal subfield to an ideal edge.

Simulation results are shown in Fig. 11. For the optimal orientation (top left), responses are a decreasing function of ξ, indicating that ξ cannot be chosen arbitrarily large. For the nonoptimal orientation (bottom left), responses are almost zero for $\xi > \approx 2$. For a more quantitative evaluation, the value of ξ is determined for which the mean nonoptimal

response of the respective noise level falls below a threshold of zero (Fig. 11, bottom right). Here, ξ depends more on the noise level than in the homogeneous case. For the highest noise level of 80%, ξ has the value of 2.01 (Fig. 11, bottom right). Because the optimal response is a decreasing function for ξ and the threshold is set to zero, the respective values of ξ also determine the maxima of the signal-to-noise ratios, i.e., the ratios of the optimal and the nonoptimal response $\bar{R}_{\text{on},90°}/\bar{R}_{\text{on},0°}$ for each noise level.

These results provide criteria for the choice of ξ. A value of $\xi \approx 2$ yields the maximal signal-to-noise ratio for the highest noise level. Since the optimal responses decrease more slowly for small noise levels, this value also results in considerably large signal-to-noise ratios for small noise levels. From the evaluation of the responses to homogeneous noise, values of ξ lie in the range $\approx [1.85; 2.25]$, depending on the noise level. Since the signal-to-noise ratios for high noise levels decrease considerably for $\xi > 2$, a value of $\xi = 2$ is chosen for the simulations (Sects. 3 and 4).

6 Discussion and conclusion

In this work, we propose a simple cell model with dominating opponent inhibition. Dominating inhibition is also used in a detailed physiological model by Troyer et al. (1998) to explain contrast invariant orientation tuning of simple cells. In contrast to our nonlinear model, Troyer et al. use linear Gabor filters to model simple cells. Strong 'antiphase' inhibition occurs between Gabor filters of phase shift 180°, i.e., opposite contrast polarity, while we employ inhibition between isotropic on and off responses. With the current physiological knowledge, evidence for both models can be found. In our model, contrast-invariant orientation tuning can be generated to a large extent by balanced inhibition at the subfield level ($\xi = 1$, Eq. 4) and by balanced inhibition between simple cells of opposite contrast polarity Eq. 6. DOI sharpens the orientation tuning and slightly increases the contrast invariance, but cannot be ascribed the primary role in generating contrast-invariant orientation tuning, as in the model of Troyer et al. Provided that intracortical recurrent interaction may also play a significant role in generating contrast-invariant orientation tuning (Adorján et al. (1999), see also Ferster and Miller (2000) for an overview) we suggest a different functional role of DOI.

Having successfully employed DOI for the simulation of physiological data on luminance gradient reversal, we then probe the model with noisy synthetic and natural im-ages. The results show that sharpness of response and robustness to noise can be increased compared to that of a model with balanced excitation and inhibition. Finally, we conduct a stochastic analysis and detailed numerical simulations to clarify the role and amount of DOI. On the basis of our findings we suggest that the visual system mainly uses dominating opponent inhibition to robustly extract oriented contrast features in noisy environments.

References

1. Adorján, P., Levitt, J.B., Lund, J.S., & Obermayer, K. (1999) A model for the intracortical origin of orientation tuning in macaque striate cortex. Vis Neurosci 16, 303–318
2. Borg-Graham, L.J., Monier, C., & Frégnac, Y. (1998) Visual input evokes transient and strong shunting inhibition in visual cortical neurons. Nature 393, 369–373
3. Ferster, D. (1988) Spatially opponent excitation and inhibition in simple cells of the cat visual cortex. J Neurosci 8(4), 1172–1180
4. Ferster, D. (1989) The synaptic inputs to simple cells in the cat visual cortex. In: Lam, D., Gilbert, C. (eds), Neural mechanisms of visual perception (pp. 63–85). The Woodlands, Texas: Portfolio
5. Ferster, D., & Miller, K.D. (2000) Neural mechanisms of orientation selectivity in visual cortex. Ann Rev Neurosci 23, 441–471
6. Hammond, P., & MacKay, D. (1983) Influence of luminance gradient reversal on simple cells in feline striate cortex. J Physiol 337, 69–87
7. Heggelund, P. (1981) Receptive field organization of simple cells in cat striate cortex. Exp Brain Res 42, 89–98
8. Heggelund, P. (1986) Quantitative studies of enhancement and suppression zones in the receptive field of simple cells in cat striate cortex. J Physiol 373, 293–310
9. Hirsch, J.A., Alonso, J.M., Reid, R.C., & Martinez, L.M. (1998) Synaptic integration in striate cortical simple cells. J Neurosci 18, 9517–9528
10. Hubel, D.H., & Wiesel, T.N. (1962) Receptive fields, binocular interaction and functional architecture in the cat's visual cortex. J Physiol 160, 106–154
11. Neumann, H., Pessoa, L., & Mingolla, E. (1998) A neural architecture of brightness perception: Non-linear contrast detection and geometry-driven diffusion. Image Vision Comput 16, 423–446
12. Neumann, H., Pessoa, L., & Hansen, T. (1999) Interaction of ON and OFF pathways for visual contrast measurement. Biol Cybern 81, 515–532
13. Palmer, L.A., & Davis, T.L. (1981) Receptive field structure in cat striate cortex. J Neurophysiol 46, 260–276
14. Papoulis, A. (1965) Probability, random variables and stochastic processes. McGraw-Hill, New York
15. Pessoa, L., Mingolla, E., & Neumann, H. (1995) A contrast- and luminance-driven multiscale network model of brightness perception. Vision Res 35, 2201–2223
16. Troyer, T.W., Krukowski, A.E., Priebe, N.J., & Miller, K.D. (1998) Contrast-invariant orientation tuning in cat visual cortex: thalomocortical input tuning and correlation-based intracortical connectivity. J Neurosci 18, 5908–5927